CNTs induced irregular 2D nanosheet SnS composites as active materials of electrodes for capacitive deionization

Pengxiao Liu*, Ling Feng, Jing Lu, Ying Li, Bin Hou, Zhumei Sun, Xu Wang

School of Environment and Safety Engineering, North University of China, Taiyuan 030051, China, Tel. +86-0351-3920588; emaila: lpx@nuc.edu.cn (P. Liu), Lynnfengling@163.com (L. Feng), 46467268@qq.com (J. Lu), 786370884@qq.com (Y. Li), 120576918@qq.com (B. Hou), 532769053@qq.com (Z. Sun), wangxuwx6@126.com (X. Wang)

ABSTRACT

Tin disulfide/carbon nanotubes (SnS/CNTs) composites have been prepared through a solvothermal method with the purpose of being used as active materials of electrodes for capacitive deionization (CDI). SnS/CNTs composites with different CNTs content (0, 5, 10, 15, and 20 wt.%) were prepared and analyzed through X-ray diffraction, scanning electron microscopy, and nitrogen adsorption and desorption measurement. Results revealed that the role of CNTs added during the synthetic reactions was more than a network facilitating the distribution of SnS, but also a kind of matter inducing a change in the morphology and pore structure of SnS during its crystallization. Compared with a cluster-like morphology of pure SnS, an irregular 2D nanosheet SnS was observed in SnS/CNTs composites, especially for SnS/CNTs-10% composite. This composite exhibited an enlarged specific surface area and a more homogeneous distribution of mesopores. Furthermore, a relatively high specific capacitance of 68.1 F/g and low resistance were verified for SnS/CNTs-10% composite. Results of desalination performance demonstrated that SnS/CNTs-10% composite electrode showed a favorable desalination capacity of 7.83 mg/g. The introduction of CNTs during SnS preparation generated a novel 2D nanosheet structure of SnS which improved the desalination performance and could be a potential material for CDI electrodes.

Keywords: Capacitive deionization; SnS; SnS/CNTs composites; Electrodes; Electrosorption

1. Introduction

With the natural freshwater resources becoming increasingly scarce, brackish water, and seawater desalination appears to be one of the strategic solutions to solve this crisis [1]. In the past decades, desalination technologies, such as reverse osmosis (RO) [2], electro dialysis (ED) [3,4], multi stage flash (MSF) [5], and multi effect distillation (MED) [6], etc., have been used to generate fresh water around the world [7]. However, high energy consumption inevitably impedes their extensive application [8]. Alternative less

energy intensive technologies have been explored and studied globally. Capacitive deionization (CDI) is one of novel desalination technologies with the merit of low energy consumption, atmospheric pressure, and environmentally-friendly characteristics, which evokes wide attention in recent years [8–10].

CDI technology is known as electrosorption technology (EST) [11]. When a low direct current potential (<2 V) is supplied between two electrodes, the ions in solution move toward the electrodes surfaces with opposite charge due to the electrostatic force, which leads to the storage of ions as

---

* Corresponding author.

the electrical double layers formed between the electrode and the electrolyte interface [12]. Thus, the ions are removed from the water, achieving desalination and purification of the brine. It is worth noting that the electrosorption capacity highly depends on the physical properties and structures of the electrode materials, such as surface areas, electrical conductivity, pore size of the porous structure, etc [13]. An excellent electrode should have high conductivity, large specific surface area, low resistance, adequate wettability, low cost, and chemical stability [11,14]. Various types of carbon materials, such as activated carbons (ACs), activated carbon fibers (ACFs), carbon aerogels (CAs), carbon nanotubes (CNTs), ordered mesoporous carbons (OMCs), etc., are applied for preparation of electrodes of CDI due to their high surface area, good conductivity, and adequate pore size [15].

Furthermore, all kinds of carbon composite materials by incorporation of other materials have been investigated, including carbon–carbon composites, such as, Gupta et al. [16] prepared the graphene-based aerogels with carbon nanotubes composite that applied as CDI electrode demonstrating ultrahigh desalination performance. Moreover, composite with different kinds of carbon materials and metal oxides [7], such as AC-MnO_2 [17], AC-TiO_2 [18], etc., have been studied. In addition, materials with superior capacitive performance for supercapacitors are also attracted widely attention and selected to apply to the CDI electrodes. For example, Hota et al. [19] synthesized the MoS_2-RGO composite for supercapacitor showing high specific capacitance properties, therefore, which providing a new way to combine metal sulfide with carbon materials for CDI application. Tian et al prepared [20] the MoS_2/g-C_3N_4 composite with a high supercapacity performance as the CDI electrode exhibiting excellent electrosorption capacity. Nevertheless, there is a lot of room for developing novel electrode materials having excellent electrosorption properties [21].

SnS is an orthogonal IV–VI group semi-conductor material with high conductivity (0.193–0.0083 S/cm) [22,23], and it is environmentally-friendly [23]. Moreover, orthorhombic SnS has a unique two-dimensional layered structure exhibiting a large interlayer spacing, which is beneficial to the transport of Na ion [24]. It has gained increasing attention in many fields as active materials [25], such as photovoltaic material [26], anode of lithium-ion battery [27], and supercapacitor [28], etc. Jayalakshmi et al. [29] found that nano SnS as electrode active material for supercapacitor had good cycling stability and the capacitance was notably improved in alkaline and neutral electrolytes [22]. Cho et al. [30] reported that SnS as one of effective sodium storage candidates could accommodate the volume changes to some extent [31]. However, to the authors' knowledge, few studies investigated the potential application of SnS as electrode active material for CDI processes.

In this study, it was attempted to apply SnS as electrode active material to fabricate electrodes for CDI. And to enhance the electrode performance, CNTs were employed to intercalate SnS in order to form SnS/CNTs composite architectures, in which CNTs were designed to increase the conductivity and inhibit the aggregation of SnS. Moreover, unexpectedly, the role of CNTs in this composite was more than that, which was observed after the relevant experiments. It was found that the morphology of SnS was changed when CNTs were introduced during the synthetic reactions. Different additive amount could result in varied pore structures of SnS/CNTs composite. Furthermore, the desalination properties, regenerability, and stability of CDI electrodes using SnS/CNTs composite as active material were investigated.

2. Experimental

2.1. Materials and reagents

Tin (II) chloride dihydrate ($SnCl_2 \cdot 2H_2O$), thiourea (CH_4N_2S), sodium citrate ($Na_3C_6H_5O_7 \cdot 2H_2O$), sodium chloride (NaCl) were gained from the Kermel Chemical Reagent Co., Ltd. (China). Ethanol, *N*-methyl-2-pyrrolidone (NMP), ethyleneglycol (EG) was supplied by the Sinopharm Chemical Reagent Co., Ltd. (China). Graphite paper was purchased from Beijing crystal special carbon technology company, China. Multi-walled Carbon nanotubes (MWCNTs) were gained from Shenzhen Turing Evolution Technology Co., Ltd. (China). Polyvinylidene fluoride (PVDF) and acetylene black (Super-P) were obtained from Arkema Chemical Reagent Co., Ltd. (France). Deionized water was used in all the experiments. All reactants and solvents were of analytical grade.

2.2. Methods

2.2.1. Preparation of SnS and SnS/CNTs composite

SnS and SnS/CNTs composite were synthesized by a solvothermal reaction. The method was based on the one reported by Chen et al. [32] with some modification. Firstly, various quantities of CNTs (0, 5, 10, 15, and 20 wt.%) were dissolved into 37 mL of EG, and the mixtures were treated by ultrasonication for 1 h. Then, 282.21 mg $SnCl_2 \cdot 2H_2O$ (1.25 mmol), 285.45 mg CH_4N_2S (3.75 mmol), and 367.63 mg sodium citrate (1.25 mmol) were added into the CNTs suspension under vigorous magnetic stirring to form an even solution. After stirring, the mixture was transferred to a 50 mL Telfon-lined sealed autoclave, followed by solvothermal treatment at 190°C for 19 h. Lastly, the products were cooled to room temperature and collected through centrifugation. The obtained products were repeatedly washed with deionized water and ethanol for three times, then dried at 60°C for 10 h to obtain the SnS or SnS/CNTs composite products.

2.2.2. Fabrication of electrodes

The electrodes were fabricated by mixing SnS/CNTs composite (80 wt.%), Super-P (10 wt.%), and PVDF (10 wt.%). The mixtures were ground in an agate mortar for 30 min, and then NMP solvent was added to form a homogeneous slurry. After that, the electrode materials were coated on one side of the graphite paper to form a thickness of 250 μm using an applicator, then cut into 5 cm × 5 cm square area. Subsequently, the electrodes were dried at 60°C for 12 h to remove the residual organic solvent. The total mass of electrode material on the graphite paper of was 50 mg.

2.2.3. Capacitive deionization apparatus

A self-made CDI module was applied in the capacitive deionization experiments. The schematic diagram of the process and structure of CDI cell are shown in Fig. 1. In short, the system included a reservoir, peristaltic pump, CDI cell, DC power supply, and conductivity meter. A non-conductive spacer was employed to separate two parallel electrode sheets of the CDI cell, which prevented short circuit and allowed water to flow. The electrodes were prepared as described previously with a size of 5 cm × 5 cm. This CDI cell worked in a flow-by mode. A direct pass of down–in and up–out flow was driven by a peristaltic pump (BT100-2J, Longerpump, China). Electric field was provided by a DC power supply (VICTOR 3003A, China) worked in constant voltage model. The NaCl concentration was measured by recording the conductivity continuously at the salt solution side with a conductivity meter (DDSJ-308F, INESA Scientific Instrument Co., Ltd., China) and the relationship between conductivity and NaCl concentration was calibrated prior to the experiment.

2.2.4. Electrosorption experiments

The CDI experiments were carried out by the self-made system in a batch mode. The initial concentration and volume of NaCl solution were 100 mg/L and 50 mL, respectively. Different flow rates (5, 10, 20, 40, and 55 mL/min) and voltages (0.8, 1.0, 1.2, and 1.3 V) were employed to investigate their influence on desalinization efficiency. New electrodes were used for each experiment except for the experiments of regenerability and stability test. Before the adsorption experiment, deionized water was employed as a test solution to clean the electrodes.

2.3. Measurements

The structure and morphology of the SnS/CNTs composite materials were analyzed using an X-ray diffraction (XRD) meter with a scan rate of 2°1/min (PXRD, TD-3700, 10 KV, CuKαradiation (λ = 2.54046 Å)) and a field emission scanning electron microscopy (SEM, Hitachi S-4800). Nitrogen adsorption and desorption isotherms were measured at 77 K on a Quantachrome Autosorb-iQ-AG instrument. The samples were degassed in vacuum at 463 K for 6 h prior to measurement. The specific surface area and pore volume was calculated using the Brunauer–Emmett–Teller (BET) method and Barrett–Joyner–Halenda (BJH) model was employed to acquire the desorption branches of isotherms so as to detect the pore size distributions.

The NaCl concentration was calculated according to the measured conductivity. The electrosorption capacity of electrodes (q, mg/g) was calculated using the following equation:

$$q = \frac{(C_0 - C_e) \cdot V}{m} \tag{1}$$

where C_0 (mg/L) and C_e (mg/L) are the initial and equilibrated NaCl concentration, respectively. V (L) is the volume of NaCl solution and m (g) is the mass of the active materials.
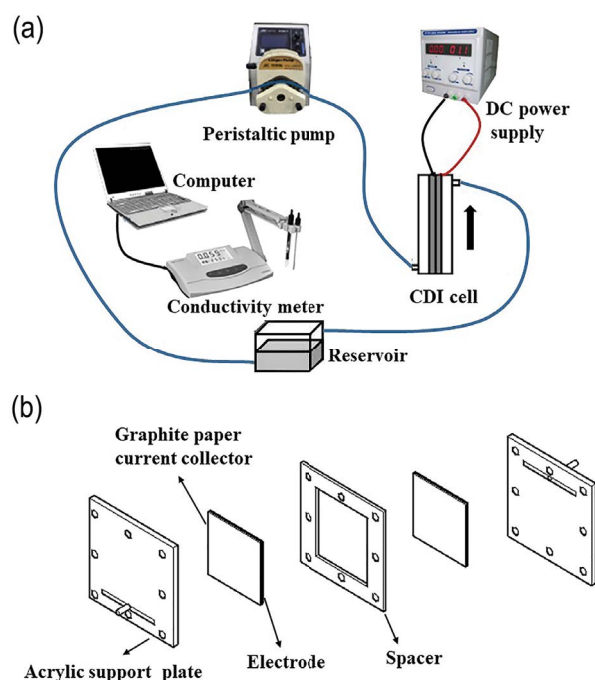

Fig. 1. Schematic diagram of the batch experiment of CDI process (a) and CDI cell structure (b).

The electrochemical measurements were conducted on an electrochemical workstation (CHI660E, Chenhua, China) with a three-electrode system in 1 M NaCl aqueous solution at room temperature. The SnS/CNTs composite with different contents of CNTs (0, 5, 10, 15, and 20 wt.%) electrodes were used as working electrodes. The platinum (Pt) plate and saturate calomel electrode (SCE) were, respectively, used as counter and reference electrode.

Cyclic voltammetry (CV) measurements were conducted in the potential range from −0.2 to 0.8 V at different scan rate (5, 10, 20, 50, and 100 mV/s). The specific capacitance was obtained through Eq. (2). Electrochemical impedance spectroscopy (EIS) tests were taken in the frequency range from 10^{-2} to 10^5 Hz with a 5 mV AC voltage around the equilibrium potential (0 V). Galvanostatical charge–discharge (GCD) were tested in the range of −0.1 to 1.0 V with a 200 mA/g current density on a LAND (Wuhan, China).

$$C = \frac{\int IdV}{2 \cdot m \cdot v \cdot \Delta V} \tag{2}$$

where C is the specific capacitance (F/g), I is the instant current (A), m is the mass of the active material (g), ΔV is the potential difference (V), and v is the potential scan rate (mV/s).

The discharge specific capacity of the electrode during galvanostatic charge–discharge measurement was calculated according to Eq. (3).

$$C_g = \frac{I_m \times \Delta t}{\Delta V} \tag{3}$$

where C_g is the capacitance (F/g), I_m is the current density (A/g), Δt is the discharge time (s), and ΔV is the potential change in discharge without the portion of iR drop (V).

3. Results and discussion

3.1. Structure and morphology of SnS/CNTs composite

Fig. 2 shows the XRD patterns of the as-prepared SnS and SnS/CNTs composite. For SnS samples, a strong preferential orientation peak centered at 32.6° can be assigned to SnS according to the normal JCPDS data. The other peaks observed at 2θ values of 22.01°, 27.47°, 39.05°, 45.50°, 48.51°, and 56.68° are matched well with orthorhombic SnS (Space group: Pbnm, JCPDS No.39-0354, lattice constants of a = 4.329 Å, b = 11.192 Å, and c = 3.984 Å), indicating the successful synthesis of SnS. The SnS/CNTs composite with various content of CNTs exhibit almost similar broad diffraction peaks as pure SnS except for that at 2θ value of 25.54°, which could be ascribed to the plane (002) of CNTs [32,33]. Hence, it can be deduced that SnS retained well when CNTs were introduced to the composite materials during the solvothermal reaction.

The morphologies and pore structures of SnS and SnS/CNTs composite were characterized using SEM. As shown in Fig. 3, the pure SnS sample exhibits a cluster-like morphology with the aggregation of nanoparticles. For SnS/CNTs composite, it was interesting to observe that the morphologies and pore structures of SnS in the composite were changed compared with those of pure SnS. It appeared that the role of CNTs added during the synthetic reactions was more than a network facilitating the distribution of SnS, which was the incipient conception before experiments, but also a kind of matter affecting the morphology of SnS during its crystallization. With the addition of CNTs, a morphology of irregular two-dimensional (2D) nanosheet of the synthesized SnS was formed in the SnS/CNTs composite, which exhibited a quite different morphology compared with the

cluster-like one of pure SnS. It could be observed for all the SnS/CNTs composite (CNTs amount of 5, 10, 15, and 20 wt.%) samples but accompanied with diversity. For SnS/CNTs-5% composite, the SnS nanosheets seemed to be comparatively thick and agminated, and CNTs did not form a clear network among the composite. For SnS/CNTs-10% composite, the SnS nanosheets were relatively thin and disperse while the CNTs were interspersed between the nanosheets forming a network, which facilitated the looseness and porousness of the composite. However, with the increase of CNTs additive amount (15% and 20%), SnS became agminated probably because of the congested CNTs. It seemed that an appropriate CNTs content was necessary to not only facilitate the formation of the ultra-thin nanosheets of SnS, but also promote the distribution of SnS nanosheets on the CNTs backbone, which were beneficial to the porousness of the composite thus convenient to the transport and adsorption of ions during CDI processes.

Fig. 4 shows the N_2 adsorption–desorption isotherms and pore size distribution of SnS and SnS/CNTs composite. The data are summarized in Table 1. Based on the IUPAC classification, all the samples exhibit a typical IV isotherm profile with a H_3 hysteresis loop, which indicates a mesoporous structure of materials. Particularly, according to the previous report [34], the H_3 hysteresis loop at high relative pressure of 0.8–1.0 for the SnS/CNTs-10% composite is typically related to adsorption within aggregates of plate-like particles, which is in accordance with the observation by SEM. Table 1 shows that the SnS/CNTs-5% composite and SnS/CNTs-10% composite possess a relatively large specific surface area and the pore volume, which can provide more adsorption sites and shorten ions diffusion length during the CDI process. As shown in Fig. 4b, there is a concentrated distribution of pore size at 3–4 nm for the SnS/CNTs-10% composite suggesting a homogeneous distribution of the mesopores, which can contribute to the transmission and adsorption performance of ions [35]. The above results reveal that both the pore structure and pore diameter distribution of the active materials have been changed by addition of CNTs.
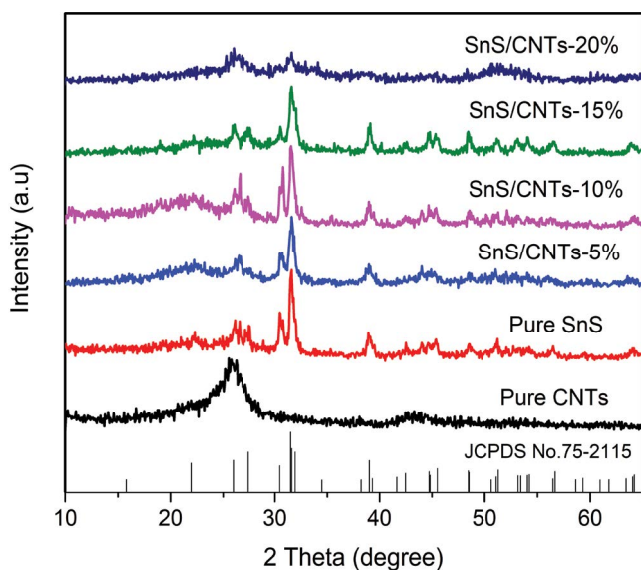
3.2. Electrochemical characteristics of SnS and SnS/CNTs composite electrodes

Electrochemical characteristics of the prepared electrodes with different active materials were firstly investigated using CV measurement at a scan rate of 5 mv/s in the potential window ranging from –0.2 to 0.8 V in 1 M NaCl solution. And the specific capacitance of all the electrodes were calculated according to the CV results. As shown in Fig. 5a, the specific capacitance of the electrodes shows a trend of increasing initially and decreasing afterwards as the increase of CNTs content. The SnS/CNTs-10% composite electrode shows a largest specific capacitance of 68.1 F/g. This result was in accordance with the previous ones of SEM, BET, and pore diameter distribution measurement.

Secondly, EIS was employed to evaluate the electrical resistance and capacitive behavior of the electrodes. The Nyquist plots of the fabricated SnS/CNTs composite electrodes materials are illustrated in Fig. 5b. The plots include two parts between Z′ (real axis) and Z″ (imaginary axis),

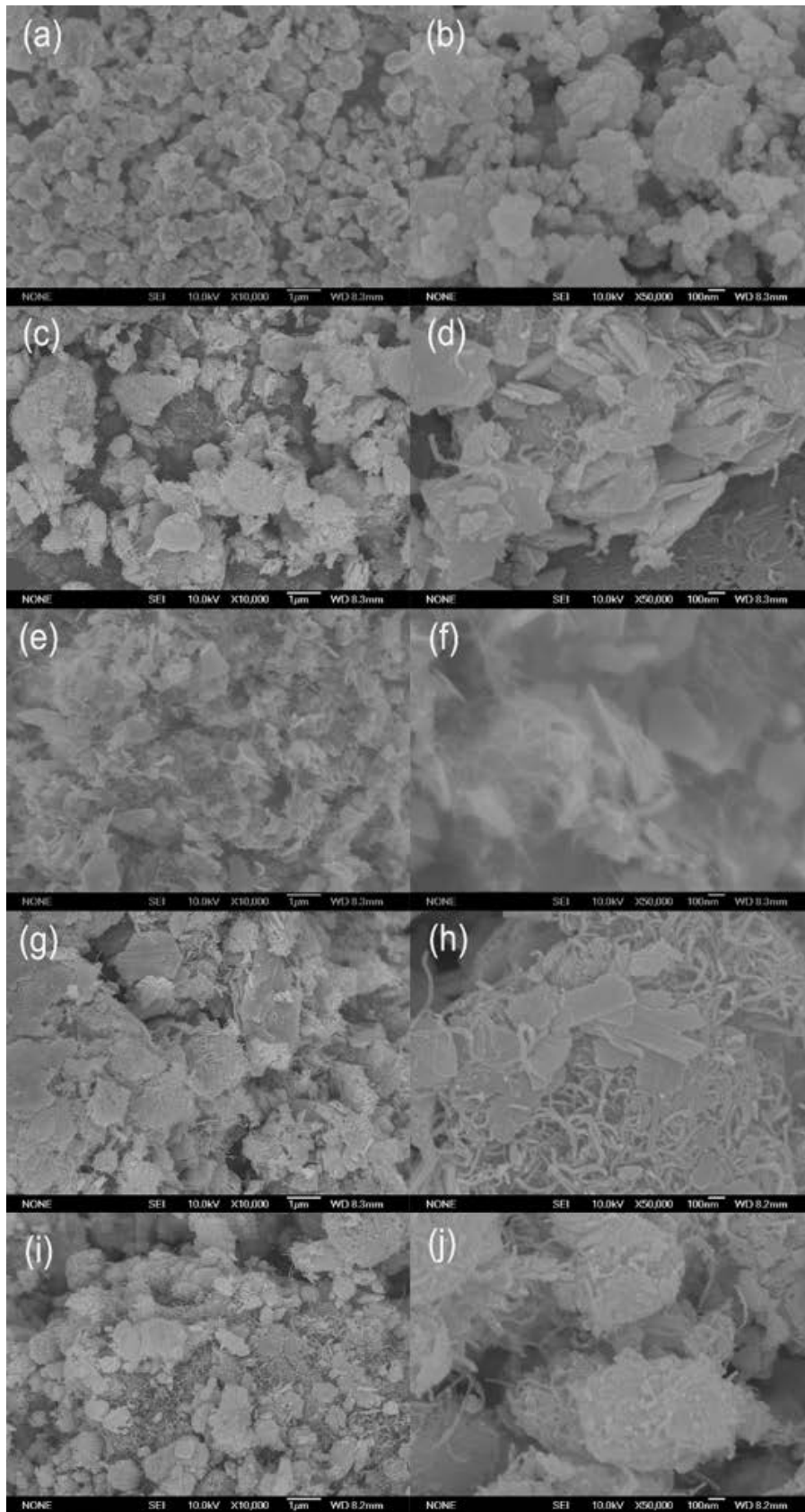Fig. 2. XRD pattern of the SnS/CNTs composite with different contents of CNTs and pure CNTs.

Fig. 3. SEM images of the SnS/CNTs composite with various CNT contents ((a and b) pure SnS, (c and d) SnS/CNTs-5%, (e and f) SnS/CNTs-10%, (g and h) SnS/CNTs-15%, (i and j) SnS/CNTs-20%).
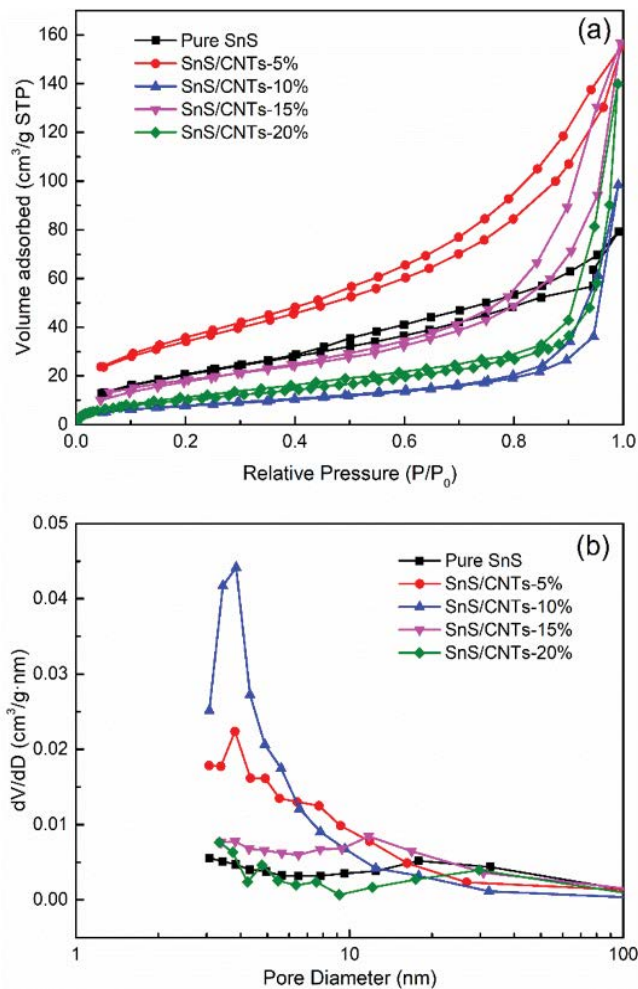
Fig. 4. N₂ adsorption–desorption isotherms (a) and BJH pore size distribution of SnS and SnS/CNTs composites (b).

Table 1
Characterization of specific surface area, pore volume, and pore size of pure SnS and SnS/CNTs composites

Sample	S_{BET} (m²/g)	D (nm)	V_{total} (m³/g)
Pure SnS	28.50	3.07	0.11
SnS/CNTs-5%	126.02	3.81	0.24
SnS/CNTs-10%	78.01	3.85	0.15
SnS/CNTs-15%	67.14	11.74	0.24
SnS/CNTs-20%	30.14	3.34	0.22

S_{BET}: special surface area calculated from BET method; D: average pore diameter; V_{total}: total pore volume.

which are a linear part of the low frequency region and a semicircle in the high frequency region. In the low frequency part, the SnS/CNTs-10% composite electrode shows a larger slope, implying an approximately ideal capacitive behavior. In the high frequency part, the intersection of the semicircle on the Z′ axis represents the equivalent series resistance (ESR) of electrodes, which includes the electronic resistance of electrodes, interfacial resistance,
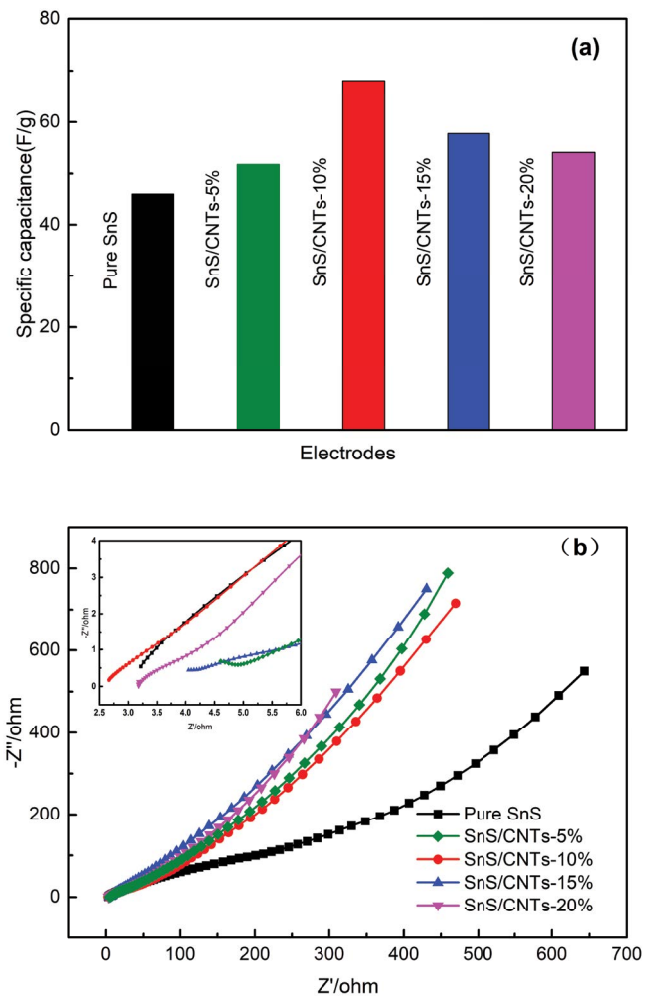

Fig. 5. Specific capacitances of the SnS/CNTs composite electrodes (a) and Nyquist impedance plots for the SnS/CNTs composite electrodes (b) (experiments conditions: at a scan rate of 5 mv/s, in a 1 M NaCl solution).

and diffusion resistance of ions [36,37]. A relatively low ESR of the SnS/CNTs-10% composite electrode (Fig. 5b inset) implies a low resistance, thus a low energy cost [38]. In conclusion, the electrochemical characteristics of electrodes are largely dependent on the characteristics of the active materials, such as morphology, surface area, pore structure, diameter distribution, and so on. In our study, the SnS/CNTs-10% composite showed a more favorable performance as active materials for CDI electrodes.

3.3. Capacitance characteristics of the SnS/CNTs-10% composite electrode

To further evaluate the capacitance characteristics of the SnS/CNTs-10% composite electrode, more tests were conducted. Fig. 6a shows the CV measurement at various scan rates in 1 M NaCl solution. As can be seen, all curves have no redox peaks in the uniform voltage window (–0.2 to 0.8 V), which indicates that ions are adsorbed to the electrodes via electrosorption rather than electrochemical
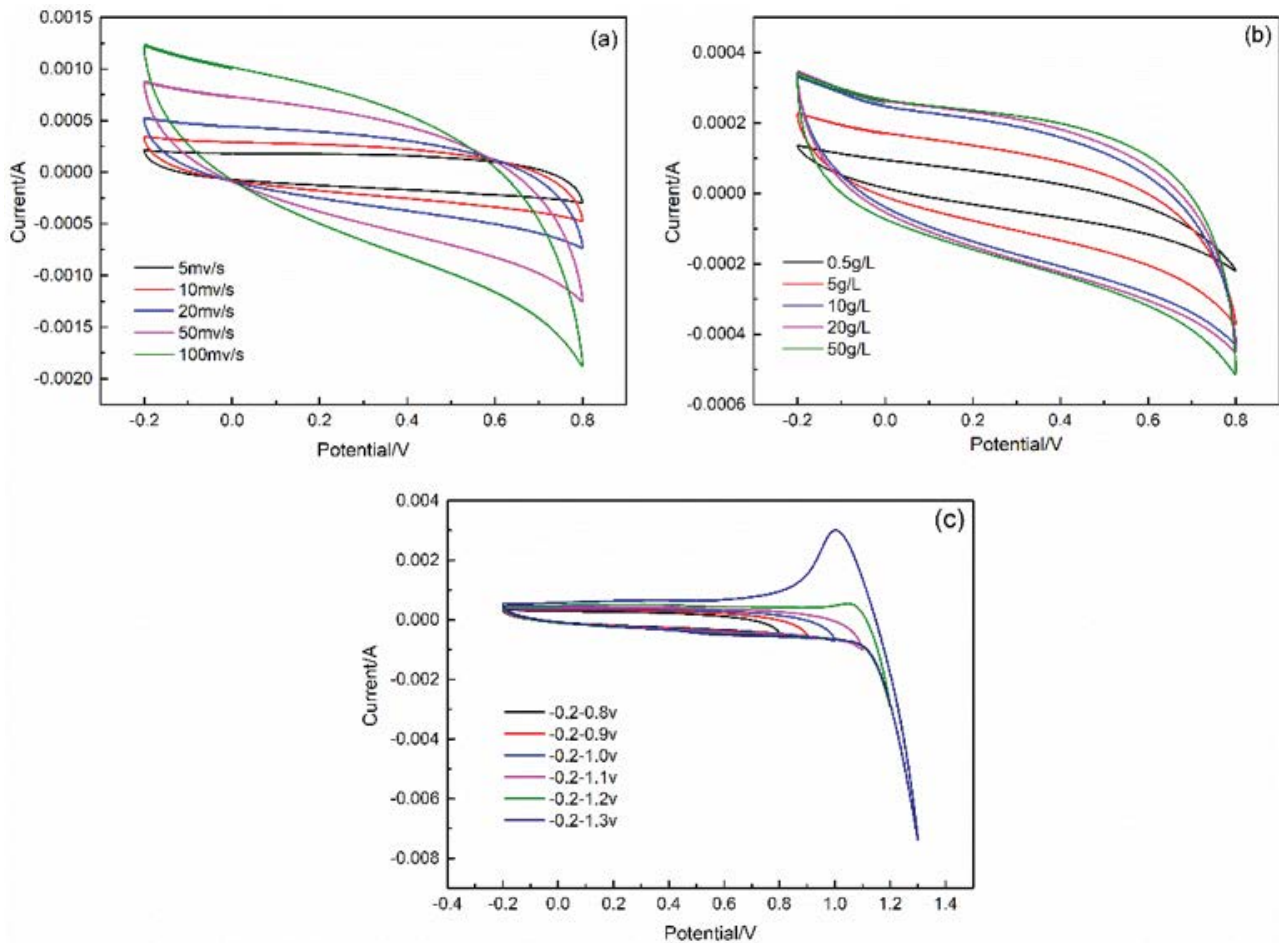
Fig. 6. CV curves of the SnS/CNTs-10% composite electrode at various scan rates (a), various NaCl concentrations (b), and various voltage ranges (c) (experiments conditions: in a 1 M NaCl solution, at a scan rate of 10 mv/s (b and c)).

reaction. The shape of curves was almost rectangular under the scan rates of 5–20 mV/s indicating an ideal double layer capacitive behavior [39], while obvious deviation occurred with the increase of scan rate to 50 and 100 mV/s. This deviation could be attributed to the inherent resistivity of the electrodes and polarization effects [8].

The relationship between solution concentration and electrosorption performance was investigated through CV measurement at a scan rate of 10 mv/s in 1 M NaCl solution as well (Fig. 6b). No electrochemical reaction occurred during the test with various concentrations of NaCl solution (0.5, 5, 10, 20, and 50 g/L). It could be observed that the induced current increased with the increasing NaCl concentration in the low value range (0.5, 5, and 10 g/L), but kept stable in the relatively high concentration range (10, 20, and 50 g/L). The reason for this phenomenon was that more ions could be accumulated on the surface of the electrodes in a higher NaCl concentration. However, if the concentration of solution was high enough, the electrode surface could be rapidly saturated and the total capacity reaches a plateau thus not further increasing [40].

The influence of voltage window on the electrosorption performance of SnS/CNTs-10% composite electrodes was also studied. As shown in Fig. 6c, at a scan rate of 10 mv/s

with different voltage range of (–0.2 to 0.8), (–0.2 to 0.9), (–0.2 to 1.0), (–0.2 to 1.1), (–0.2 to 1.2), and (–0.2 to 1.3) V in 1 M NaCl solution, the total capacity increased with the increasing voltage implying the significance of voltage impact. However, it was noteworthy that remarkable peaks were observed when the applied voltage was in the range of –0.2 to 1.3 V, which indicated Faradaic reactions occurred and became significant. Therefore, it could be deduced that 1.2 V was a threshold value of applied voltage to keep a stable capacity of electrosorption for the SnS/CNTs-10% composite electrodes.

The galvanostatic charge–discharge characteristics of the SnS/CNTs-10% composite electrodes was investigated at a constant current load of 200 mA/g and voltage range between –0.1 and 1.0 V in 1 M NaCl solution. As shown in Fig. 7a, typical isosceles triangles can be observed for the charge–discharge curve, which demonstrates the good reversibility and ideal capacitance behavior with no occurrence of Faradaic reactions [41]. The discharge specific capacity of the electrode was calculated according to Eq. (3). It was 143.17 F/g for the SnS/CNTs-10% composite electrode and 96.33 F/g for pure SnS electrode, which demonstrated an excellent capacitance characteristic of the former, and the result was in accordance with that of

the previous CV measurement. Besides, the attenuation of charge and discharge was not observed and the curve retained triangular shape after 50 cycles (Fig. 7b), reflecting the good stability and cycling performance of the SnS/CNTs-10% composite electrode.

3.4. CDI performance of the SnS/CNT composite electrode

After the electrochemical characteristic measurement, desalination capacity of the SnS/CNTs composite electrode was tested. Firstly, the SnS/CNTs-10% composite electrode was selected to optimize the operating parameters of CDI process since it was speculated that this electrode could be the preferable one according to the previous tests. Thus, different flow rates and voltage were investigated through single factor tests.

Desalination experiments with different flow rates (5, 10, 20, 40, and 55 mL/min) were conducted with an initial NaCl concentration of 100 mg/L and applied voltage of 1.2 V. The change of conductivity of the NaCl solution with time and the calculated electrosorption capacity of the electrode after achieving the adsorption equilibrium were shown in Fig. 8. It was interesting to find that the electrosorption capacity was enhanced with the increased flow rate from 5 to 20 mL/min while it was reduced with the further increase from 20 to 55 mL/min. The flow rate of 20 mL/min seemed to be the optimum value for achieving a favorable desalination performance with an electrosorption capacity value of 8.10 mg/g. Higher flow rate could promote the mass transfer thus facilitating the migration of ions from bulk solution to boundary layers and leading to the increased adsorption [42]. However, with the further increase of flow rate, less retention time for ion migration conversely led to the decrease of adsorption [43]. Besides, high flow rate could generate strong shearing force thus disturbing the ions adsorbed on the electrode surface due to the electrostatic force. Similar results were obtained in the previous study [38].

Different voltage (0.8, 1.0, 1.2, and 1.3 V) was applied to investigate its influence to the desalination performance of the SnS/CNTs-10% composite electrode. As shown in Fig. 9a, the electrosorption capacity was enhanced with the increased voltage except for that of 1.3 V. The decreased electrosorption capacity at 1.3 V (4.89 mg/g) compared with that at 1.2 V (7.83 mg/g) could result from the occurrence of Faradic reaction that largely consumed the electric energy. Similar results were also obtained in previous study [44]. Therefore, 1.2 V was a favorable potential for the CDI process in this study. Electrosorption stability of the SnS/CNTs-10% composite electrode was also investigated by repeating adsorption–desorption processes with an initial NaCl concentration of 100 mg/L, flow rate of 20 mL/min, and applied voltage of 1.2 V. As shown in Fig. 9b, after three times of adsorption–desorption cycles, the electrosorption capacity remained stable, suggesting a good electrosorption stability of the electrode in the CDI processes.

Furthermore, to verify the assumption that the SnS/CNTs-10% composite electrode was the preferable one, desalination behavior of all the prepared SnS/CNTs composite electrodes were evaluated under the optimized parameters. The calculated salt adsorption capacity

according to Eq. (1) are shown in Table 2. The SnS/CNTs-10% composite electrode indeed exhibited a favorable desalination capacity (7.83 mg/g) than other electrodes. Besides, Fig. 10 shows the change of conductivity of NaCl solution with time during the desalination using SnS and SnS/CNTs-10% composite electrodes. It could be observed
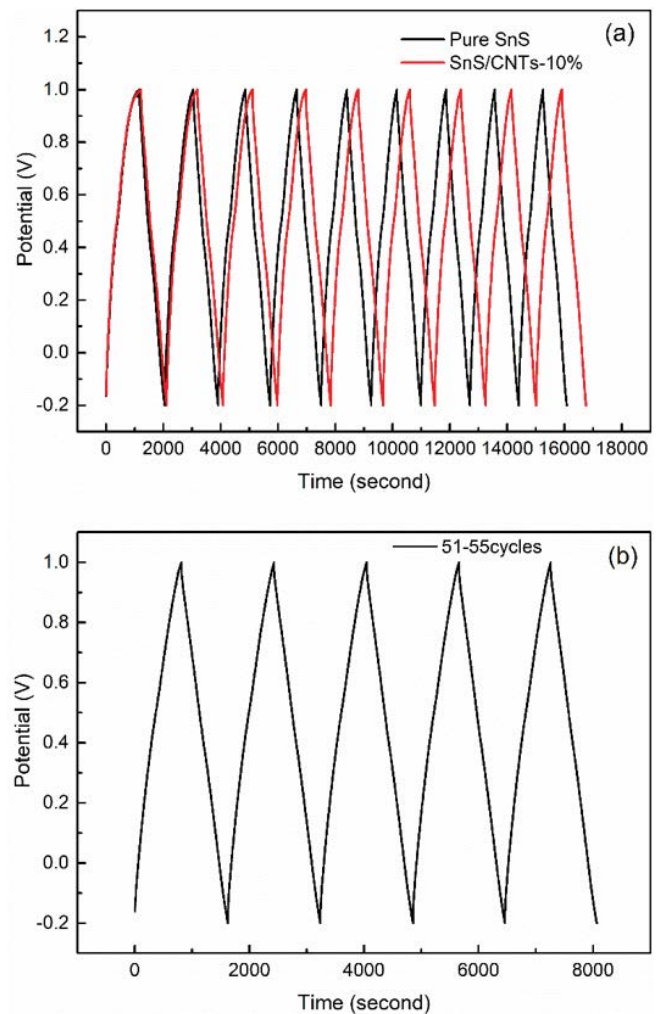

Fig. 7. Galvanostatic charge/discharge curves of pure SnS and SnS/CNTs-10% composite electrodes (a); and galvanostatic charge/discharge curves of SnS/CNTs-10% electrodes after at least 55 cycles (b) (experiments conditions: at a constant current load of 200 mA/g, voltage of –1.0 to 1.0 V, in a 1 M NaCl solution).

Table 2
Electrosorption capacity of SnS/CNTs composite electrodes

Electrodes	Electrosorption capacity (mg g^{-1})
Pure SnS	3.13
SnS/CNTs-5%	3.59
SnS/CNTs-10%	7.83
SnS/CNTs-15%	2.23
SnS/CNTs-20%	3.49

that the conductivity of NaCl solution decreased rapidly and became stable after around 10 min for the desalination using SnS electrode while it decreased moderately and got steady after around 70 min for the case of SnS/CNTs-10% composite electrode. The phenomenon could be ascribed to the diversity of the electrosorption capacity of the two electrodes, which derived from the substantial difference of the morphology and pore structure of the active materials of electrodes. As discussed previously, the irregular 2D nanosheets of SnS in SnS/CNTs-10% composite were more beneficial to form a porous structure than the cluster-like pure SnS. Besides, CNTs as backbones that were interspersed between the SnS nanosheets facilitated the distribution of the nanosheets to form a loose and porous structure, which enhanced the specific surface area and benefited for reducing the pathway of Na^+ and Cl^- diffusion during CDI as well.

4. Conclusion

In this work, SnS/CNTs composites were fabricated successfully and applied as active materials of electrodes for CDI. Different CNTs content (0, 5, 10, 15, and 20 wt.%)

was introduced into the solvothermal reaction for SnS synthesis. The successful synthesis of SnS in both pure SnS and SnS/CNTs composites samples were verified through XRD. And through SEM and nitrogen adsorption and desorption measurement, it was found that CNTs added during the synthetic reactions not only facilitated the distribution of SnS as a network but also induced a change in the morphology and pore structure of SnS during its crystallization. An irregular 2D nanosheet SnS have been observed in SnS/CNTs composites, especially for SnS/CNTs-10% composite, compared with a cluster-like morphology of pure SnS. In addition, a relatively high specific capacitance of 68.1 F/g and low resistance were verified for the SnS/CNTs-10% composite electrode through CV and EIS measurements. Finally, it was further demonstrated that the SnS/CNTs-10% composite electrode exhibited a favorable desalination capacity of 7.83 mg/g. It was the novel 2D nanosheet structure of SnS in the SnS/CNTs-10% composite that led to the improvement of the desalination performance and it could be a potential material for CDI electrodes.
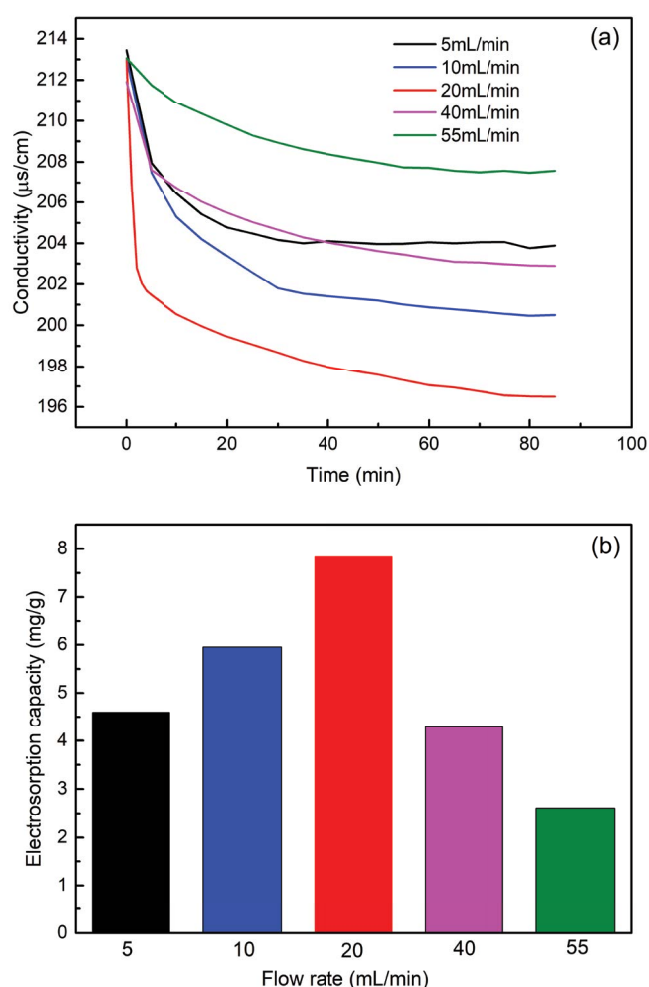

Fig. 8. Conductivity change during CDI using SnS/CNTs-10% composite electrodes at different flow rates (a) and corresponding electrosorption capacities (b).
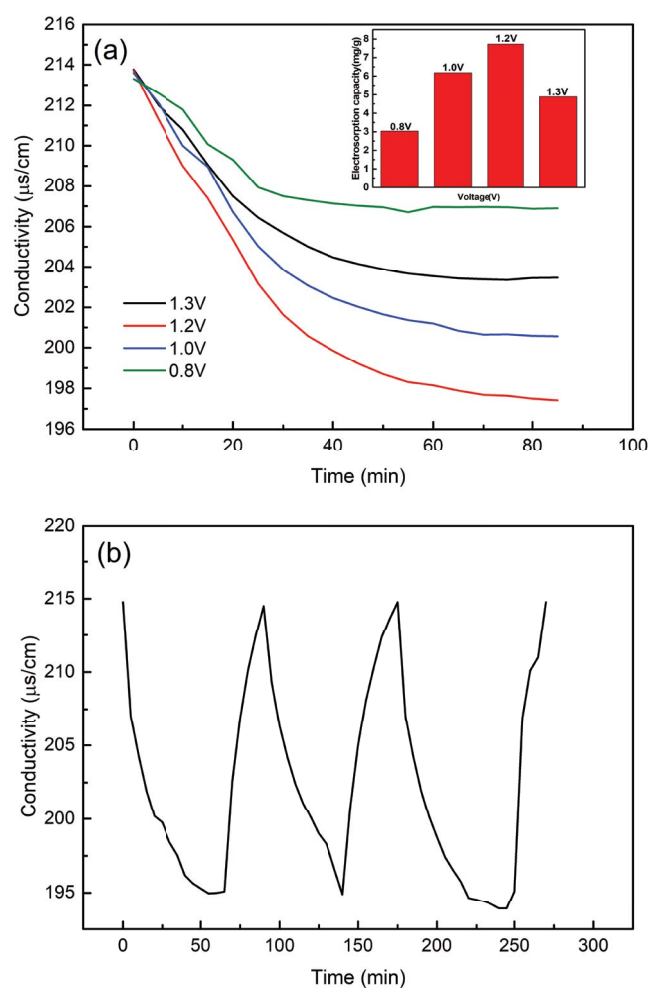

Fig. 9. Conductivity change during CDI using SnS/CNTs-10% composite electrodes under different voltages (a) and the cycling stability (b) (experiments conditions: in a 100 mg/L NaCl solution, at the flow rate of 20 mL/min).
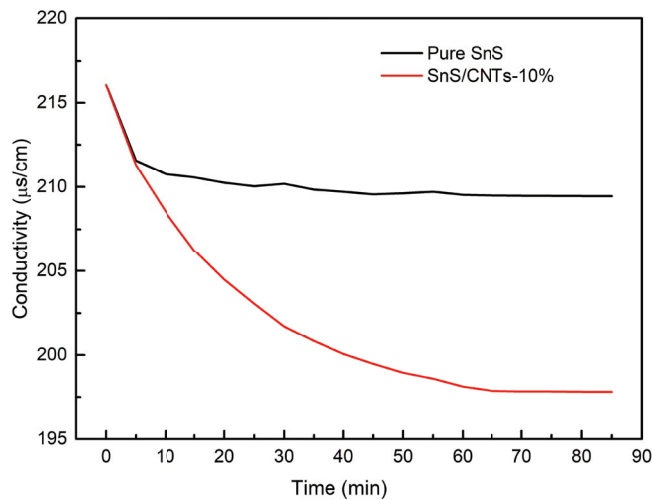
Fig. 10. Conductivity change during CDI using SnS and SnS/CNTs-10% composite electrodes (experiments conditions: in a 100 mg/L NaCl solution, at the flow rate of 20 mL/min, and under a voltage of 1.2 V).

Acknowledgments

References

[1] F.A. AlMarzooqi, A.A. Al Ghaferi, I. Saadat, N. Hilal, Application of capacitive deionisation in water desalination: a review, Desalination, 342 (2014) 3–15.
[2] K.P. Lee, T.C. Arnot, D. Mattia, A review of reverse osmosis membrane materials for desalination—development to date and future potential, J. Membr. Sci., 370 (2011) 1–22.
[3] M. Sadrzadeh, T. Mohammadi, Sea water desalination using electrodialysis, Desalination, 221 (2008) 440–447.
[4] H.J. Lee, F. Sarfert, H. Strathmann, S.H. Moon, Designing of an electrodialysis desalination plant, Desalination, 142 (2002) 267–286.
[5] R. Borsani, S. Rebagliati, Fundamentals and costing of MSF desalination plants and comparison with other technologies, Desalination, 182 (2005) 29–37.
[6] H.T. El-Dessouky, H.M. Ettouney, Y. Al-Roumi, Multi-stage flash desalination: present and future outlook, Chem. Eng. J., 73 (1999) 173–190.
[7] J. Oladunni, J.H. Zain, A. Hai, F. Banat, G. Bharath, E. Alhseinat, A comprehensive review on recently developed carbon based nanocomposites for capacitive deionization: from theory to practice, Sep. Purif. Technol., 207 (2018) 291–320.
[8] Z. Peng, D. Zhang, L. Shi, T. Yan, High performance ordered mesoporous carbon/carbon nanotube composite electrodes for capacitive deionization, J. Mater. Chem., 22 (2012) 6603–6612.
[9] L. Zou, L. Li, H. Song, G. Morris, Using mesoporous carbon electrodes for brackish water desalination, Water Res., 42 (2008) 2340–2348.
[10] T.J. Welgemoed, C.F. Schutte, Capacitive deionization technology™: an alternative desalination solution, Desalination, 183 (2005) 327–340.
[11] S. Porada, R. Zhao, A. van der Wal, V. Presser, P.M. Biesheuvel, Review on the science and technology of water desalination by capacitive deionization, Prog. Mater. Sci., 58 (2013) 1388–1442.
[12] F. Ahmad, S.J. Khan, Y. Jamal, H. Kamran, A. Ahsan, M. Ahmad, A. Khan, Desalination of brackish water using capacitive deionization (CDI) technology, Desal. Water Treat., 57 (2016) 7659–7666.
[13] F. Duan, Y. Li, H. Cao, Y. Xie, Y. Zhang, Capacitive deionization by ordered mesoporous carbon: electrosorption isotherm, kinetics, and the effect of modification, Desal. Water Treat., 52 (2014) 1388–1395.
[14] M.A. Ahmed, S. Tewari, Capacitive deionization: processes, materials and state of the technology, J. Electroanal. Chem., 813 (2018) 178–192.
[15] D.K. Kohli, R. Singh, M.K. Singh, A. Singh, R.K. Khardekar, P. Ram Sankar, P. Tiwari, P.K. Gupta, Study of carbon aerogel-activated carbon composite electrodes for capacitive deionization application, Desal. Water Treat., 49 (2012) 130–135.
[16] S. Gupta, A. Henson, B. Evans, R. Meek, Graphene-based aerogels with carbon nanotubes as ultrahigh-performing mesoporous capacitive deionization electrodes for brackish and seawater desalination, Desal. Water Treat., 162 (2019) 97–111.
[17] J. Yang, L. Zou, H. Song, Z. Hao, Development of novel MnO$_2$/nanoporous carbon composite electrodes in capacitive deionization technology, Desalination, 276 (2011) 199–206.
[18] C. Kim, J. Lee, S. Kim, J. Yoon, TiO$_2$ sol–gel spray method for carbon electrode fabrication to enhance desalination efficiency of capacitive deionization, Desalination, 342 (2014) 70–74.
[19] P. Hota, M. Miah, S. Bose, D. Dinda, S.K. Saha, Ultra-small amorphous MoS$_2$ decorated reduced graphene oxide for supercapacitor application, J. Mater. Sci. Technol., 40 (2020) 196–203.
[20] S. Tian, X. Zhang, Z. Zhang, Capacitive deionization with MoS$_2$/g-C$_3$N$_4$ electrodes, Desalination, 479 (2020) 1–12, doi: 10.1016/j.desal.2020.114348.
[21] Y. Wang, Y. Zhang, J. Shi, A. Pan, F. Jiang, S. Liang, G. Cao, S-doped porous carbon confined SnS nanospheres with enhanced electrochemical performance for sodium-ion batteries, J. Mater. Chem. A, 6 (2018) 18286–18292.
[22] Y. Li, H. Xie, J. Tu, Nanostructured SnS/carbon composite for supercapacitor, Mater. Lett., 63 (2009) 1785–1787.
[23] F. Wang, Q. Yao, L. Zhou, Z. Ma, M. He, F. Wu, Theoretical understanding of SnS monolayer as Li ion battery anode material, J. Phys. Chem. Solids, 121 (2018) 261–265.
[24] J. Shi, Y. Wang, Q. Su, F. Cheng, X. Kong, J. Lin, T. Zhu, S. Liang, A. Pan, N-S co-doped C@SnS nanoflakes/graphene composite as advanced anode for sodium-ion batteries, Chem. Eng. J., 353 (2018) 606–614.
[25] S. Li, J. Zheng, Z. Hu, S. Zuo, Z. Wu, P. Yan, F. Pan, 3D-hierarchical SnS nanostructures: controlled synthesis, formation mechanism and lithium-ion storage performance, RSC Adv., 5 (2015) 72857–72862.
[26] N.K. Reddy, K.T.R. Reddy, SnS films for photovoltaic applications: physical investigations on sprayed SnxSy films, Phys. B, 368 (2005) 25–31.
[27] X. Gou, J. Chen, P. Shen, Synthesis, characterization and application of SnS (=1, 2) nanoparticles, Mater. Chem. Phys., 93 (2005) 557–566.
[28] R. Barik, N. Devi, V.K. Perla, S.K. Ghosh, K. Mallick, Stannous sulfide nanoparticles for supercapacitor application, Appl. Surf. Sci., 472 (2019) 112–117.
[29] M. Jayalakshmi, M.M. Rao, B.M. Choudary, Identifying nano SnS as a new electrode material for electrochemical capacitors in aqueous solutions, Electrochem. Commun., 6 (2004) 1119–1122.
[30] E. Cho, K. Song, M.H. Park, K.-W. Nam, Y.-M. Kang, SnS 3D flowers with superb kinetic properties for anodic use in next-generation sodium rechargeable batteries, Small, 12 (2016) 2510–2517.
[31] S. Zhang, L. Yue, H. Zhao, Z. Wang, J. Mi, Mwcnts wrapped flower-like SnS composite as anode material for sodium-ion battery, Mater. Lett., 209 (2017) 212–215.
[32] Y. Chen, B. Wang, T. Hou, X. Hu, X. Li, X. Sun, S. Cai, H. Ji, C. Zheng, Enhanced electrochemical performance of SnS nanoparticles/CNTs composite as anode material for sodium-ion battery, Chin. Chem. Lett., 29 (2018) 187–190.

[33] G. Zhou, L. Li, Q. Zhang, N. Li, F. Li, Octahedral Co$_3$O$_4$ particles threaded by carbon nanotube arrays as integrated structure anodes for lithium ion batteries, Phys. Chem. Chem. Phys., 15 (2013) 5582–5587.
[34] M.A. Worsley, P.J. Pauzauskie, T.Y. Olson, J. Biener, J.H. Satcher Jr., T.F. Baumann, Synthesis of graphene aerogel with high electrical conductivity, J. Am. Chem. Soc., 132 (2010) 14067–14069.
[35] X. Liu, T. Chen, W.-C. Qiao, Z. Wang, L. Yu, Fabrication of graphene/activated carbon nanofiber composites for high performance capacitive deionization, J. Taiwan Inst. Chem. Eng., 72 (2017) 213–219.
[36] Z. Lei, N. Christov, X.S. Zhao, Intercalation of mesoporous carbon spheres between reduced graphene oxide sheets for preparing high-rate supercapacitor electrodes, Energy Environ. Sci., 4 (2011) 1866–1873.
[37] S. Dutta, S.-Y. Huang, C. Chen, J.E. Chen, Z.A. Alothman, Y. Yamauchi, C.-H. Hou, K.C.W. Wu, Cellulose framework directed construction of hierarchically porous carbons offering high-performance capacitive deionization of brackish water, ACS Sustainable Chem. Eng., 4 (2016) 1885–1893.
[38] H. Song, Y. Wu, S. Zhang, W. Li, B. Wang, C. Wang, J. Gao, A. Li, Mesoporous generation-inspired ultrahigh capacitive deionization performance by sono-assembled activated carbon/inter-connected graphene network architecture, Electrochim. Acta, 205 (2016) 161–169.
[39] N. Arora, F. Banat, G. Bharath, E. Alhseinat, Capacitive deionization of NaCl from saline solution using graphene/CNTs/ZnO NPs based electrodes, J. Phys. D: Appl. Phys., 52 (2019) 455304 1–13, doi: 10.1088/1361-6463/ab3967.
[40] K.L. Yang, T.-Y. Ying, S. Yiacoumi, C. Tsouris, E.S. Vittoratos, Electrosorption of ions from aqueous solutions by carbon aerogel? an electrical double-layer model, Langmuir, 17 (2001) 1961–1969.
[41] D. Zhang, T. Yan, L. Shi, Z. Peng, X. Wen, J. Zhang, Enhanced capacitive deionization performance of graphene/carbon nanotube composites, J. Mater. Chem., 22 (2012) 14696–14704.
[42] P. Liang, L. Yuan, X. Yang, S. Zhou, X. Huang, Coupling ion-exchangers with inexpensive activated carbon fiber electrodes to enhance the performance of capacitive deionization cells for domestic wastewater desalination, Water Res., 47 (2013) 2523–2530.
[43] K. Wei, Y. Zhang, W. Han, J. Li, X. Sun, J. Shen, L. Wang, A novel capacitive electrode based on TiO$_2$-NTs array with carbon embedded for water deionization: fabrication, characterization and application study, Desalination, 420 (2017) 70–78.
[44] C. Wang, H. Song, Q. Zhang, B. Wang, A. Li, Parameter optimization based on capacitive deionization for highly efficient desalination of domestic wastewater biotreated effluent and the fouled electrode regeneration, Desalination, 365 (2015) 407–415.